Available online at www.sciencedirect.com

ScienceDirect

Ceramics International 40 (2014) 2017–2022

CERAMICS INTERNATIONAL

www.elsevier.com/locate/ceramint

Preparation and photocatalytic activity of N–Ag co-doped TiO_2/C porous ultrafine fibers mat

Nan Wu[a], Yingde Wang[a], Yongpeng Lei[b,*], Bing Wang[a]

[a]*Science and Technology on Advanced Ceramic Fibers and Composites Laboratory, National University of Defense Technology, Changsha 410073, Hunan, PR China*

[b]*College of Basic Education, National University of Defense Technology, Changsha 410073, Hunan, PR China*

Received 16 June 2013; received in revised form 22 July 2013; accepted 23 July 2013
Available online 30 July 2013

Abstract

N–Ag co-doped TiO_2/C porous ultrafine fibers mat was prepared by a sol–gel/electrospinning process using polyacrylonitrile (PAN) as a precursor and Ti $(OC_4H_9)_4$, $AgNO_3$, urea as titanium, silver, nitrogen source, respectively. The porous structure was obtained by etching SiO_2 nano-particles. Structure and properties of the fibers mat were characterized by SEM, TEM, XRD, XPS, UV–vis, Raman spectroscopy and N_2 physical adsorption analysis. Silver ion and SiO_2 nano-particles have a great influence on the crystallization of TiO_2. The photocatalytic activity was measured by the degradation of methylene blue (MB) under visible light irradiation. N–Ag co-doped TiO_2/C fibers mat exhibited much higher photocatalytic destruction rate than P25. The photocatalytic efficiency of porous fibers mat increased by 11% after etching.

Keywords: Photocatalyst; Co-doped; Electrospinning

1. Introduction

Nano-sized TiO_2 is considered as the most superior photocatalytic material owing to its excellent properties, such as non-toxicity, structural stability, abundance, high oxidation rate and ecological friendliness [1]. It has been used in photocatalytic degradation of organic pollutants, toxic gas and disinfection of polluted water [2]. However, TiO_2 only absorbs UV light for its wide band gap of 3.2 eV and natural sunlight consists of 5% UV light (300–400 nm) [3]. Therefore, the shift of the absorption of TiO_2 from UV light region to the visible light region will have a profound effect on the photocatalytic reaction. Much progress realized the target by importing various dopants into TiO_2 lattice, including Fe, Ag, V, Cr, Co, N, C and F. The dopants of the above elements were applied to amend the electronic capability and light absorption ranges of TiO_2 [3–6]. Recently, the research on kinetics has suggested that the dopants improve the band gap of TiO_2 [7]. Doped TiO_2 exhibited greater photocatalytic activity under visible light than pure TiO_2 though the UV photocatalytic activity was relatively low in some cases. N–Fe co-doped nano-TiO_2 improved the efficiency of photocatalytic reactions by 75% and 5% under visible and UV irradiations, respectively, compared with the pure TiO_2 [2].

It is known that the photocatalytic activity is relevant to the surface area of the catalyst [8]. In the past decade, porous TiO_2 particles and fibers covered with TiO_2 have been fabricated to increase the photocatalytic efficiency [9,10]. As reported by Ming et al., TiO_2 hollow particles prepared by a hydrothermal method with the BET surface area of 117 m^2/g showed higher photocatalytic activity than P25 [11]. Chen et al. deposited TiO_2 on the activated carbon fibers (ACF) by an electrochemical method, possessing much higher photocatalytic efficiency than pristine TiO_2 [10]. Nevertheless, both porous TiO_2 particles and TiO_2/ACF composites cannot reclaim conveniently or take shape as conceived.

In the present work, we fabricated N–Ag co-doped TiO_2/C porous ultrafine fibers mat by a sol–gol/electrospinning method. The photocatalytic activity of fibers mat was evaluated by measurement of the degradation of methylene blue (MB) under visible light irradiation.

*Corresponding author. Tel./fax: +86 731 84575118.
E-mail addresses: wyd502@163.com (Y. Wang), lypkd@163.com (Y. Lei).

0272-8842/$ - see front matter © 2013 Elsevier Ltd and Techna Group S.r.l. All rights reserved.
http://dx.doi.org/10.1016/j.ceramint.2013.07.112

2. Experimental

2.1. Sample preparation

The fibers mat was synthesized by a sol–gel process combined with the electrospinning method. PAN, Ti $(OC_4H_9)_4$ and acetic acid were used as starting materials. $AgNO_3$ and urea were used as silver source and nitrogen source, respectively. The spinnable sols were prepared by the following procedures. Firstly, 1.2 g PAN was dissolved in 8.8 g N, N′-dimethylformamide (DMF) under magnetic stirring at 40 °C for 24 h (solution A). 4 g Ti $(OC_4H_9)_4$ and 0.01 g $AgNO_3$ were added into 1 ml acetic acid under magnetic stirring for 6 h (solution B). Then golden spinnable sols were obtained by adding solution B and urea into solution A under magnetic stirring for 24 h (The sols for fabricating porous fibers mat were prepared after introducing SiO_2 nano-particles into the golden sols). Finally, the golden sols were brought into the injection and connected with a thin pinhead with an inner diameter of 0.8 mm. The pinhead connecting to a high voltage of 10 KV was served as the positive electrode. The fibers were collected on the aluminum foil which was employed as the negative electrode.

The as-spun fibers mat was stabilized in an oven at 250 °C for 2 h at a heating rate of 3 °C/min. Then, it was pyrolyzed up to 600 °C at a rate of 3 °C/min in a tubular furnace under nitrogen atmosphere. To achieve the porous structure, the fibers mat consisting of SiO_2 was dipped in 10 wt% HF aqueous solution for 24 h to remove SiO_2 nano-particles. The mat was dried at 60 °C for 12 h after washing with ethanol and deionized water. Finally, the fibers mats obtained were denoted as pure TiO_2/C (TC), N-doped TiO_2/C (NTC), N–Ag co-doped TiO_2/C (NATC) and porous N–Ag co-doped TiO_2/C (PNATC).

2.2. Characterization

X-ray diffraction (XRD) patterns, collected in the range 10–70° (2θ) using Siemens D-500 diffractometer (Cu Kα radiation, $\lambda = 1.5406$ Å) working at 40 kV and 40 mA, were used to identify phase constitutions and crystallite sizes. The Raman spectra were tested (LabRAM HR, Horiba Jobin Yvon) using a 514.5 nm, air-cooled Ar^+ laser with 50× objective and with laser intensity of 1.3 mW. The data acquisition time was kept at 20 s. Scanning electron microscopy (SEM) was used to observe the section and exterior morphology of the electrospun fibers. It was recorded on JEOL JSM-6360LV which operating at 5 kV. The transmission electron microscopy (TEM) observations were obtained on a Tecnai G2 F20. Samples were added on carbon-coated copper grids before observation. The mass ratio of TiO_2 in the fibers mat was measured using a Thermo-gravimetric Analyzer Pyris 1 TGA (Perkin-Elmer); the sample was heated at 10 °C/min under air atmosphere. The X-ray photoelectron spectroscopy (XPS) spectra were obtained by means of a K-Alpha 1063 electron spectrometer using Al Kα radiation. The surface areas of the fibers mat were estimated using the Brunauer–Emmett–Teller (BET) equation (QuadraSorb Station 3) after preheating the samples at 150 °C for 3 h to eliminate the adsorbed water. Pore size distributions were obtained from the adsorption branches of isotherms by using the Barret–Joyner–Halenda (BJH) model. UV–visible diffuse reflectance spectra were obtained for the fibers mat using a Scan UV–visible spectrophotometer (U-4100, Hitachi).

2.3. Photodegradation of methylene blue

The photocatalytic activity of fibers mat was evaluated by measuring the decomposition of methylene blue with a concentration of 10 mg/L under visible-light irradiation. The visible-light source was a 1000 W halogen lamp. A colored glass filter with cut-off wavelength of 420 nm was used for eliminating UV light. For a typical photocatalytic experiment, 0.1 g of the fibers mat shaped like rectangle was added into 100 ml of the above methylene blue solution in a two neck flask. Then, the flask was installed in a thermostatic waterbath to keep the solution at 20 °C. Before the irradiation, the mixture was magnetically stirred in dark for 30 min to catch the establishment of an adsorption–desorption equilibrium. The air was immited into the admixture through an air pump to make the rectangle fibers mat rolled in the solution. After a setup exposure time, 3.0 ml mixture solution was sampled and detected by a 722S visible spectrophotometer (INESA, Shanghai) at 661 nm. For comparison, the same experiment was also done in the presence of P25 (purchased from Xiya reagent, Chengdu).

3. Results and discussion

Fig. 1 exhibits the SEM images of NATC (a, b) and PNATC (c). In Fig. 1(a), the nanofibers showed long and straight morphology with uniform diameters ranging from 350 to 450 nm. Fig. 1(b) demonstrates many grooves on the surface of NATC fibers. After etching of SiO_2 by HF, PNATC with a great number of nano-sized holes was obtained (Fig. 1c).

Fig. 2(a) presents a typical magnification TEM image of NATC, suggesting that TiO_2 nano-particles exist in the fibers well-proportioned. A HRTEM image of the sample in Fig. 2(b) showed that Ag nano-particles with the diameters of 5 nm were adhered to the surface of TiO_2. The lattice fringe spacing of 0.35 nm and 0.236 nm corresponded to the anatase-phase TiO_2 (101) plane and Ag with the cubic structure (111) plane, respectively [12].

To determine the composition of the fibers mat and confirm the valence states of various atoms, XPS analysis was carried out (Fig. 3). The binding energy of O 1s in pure TiO_2 is 529.3 eV [13]. While O 1s XPS spectrum of the NATC (Fig. 3a) was divided into two sub-peaks centered at 530.0 eV and 532.1 eV. This was contributed to the formation of O–Ti–N structure and Ti–O–N structure due to the replacement of O in TiO_2 lattice by N atoms [14]. In the Ti 2p XPS spectrum (Fig. 3b), two peaks were observed at 458.8 and 464.5 eV. They were assigned to $2p_{3/2}$ and $2p_{1/2}$ respectively, attributing to Ti^{4+} in anatase titania [15]. Fig. 3c shows the N 1s spectrum. The feature at around 397 eV was generally

considered to the formation of O–Ti–N structure resulting from substitution for oxygen sites by nitrogen atoms in the TiO_2 lattice [3,16]. Asahi et al. have definitely pointed out that the N 1s peak at 400 eV can be assigned to NO species occupying in the interstitial TiO_2 site [17]. Gole et al. prepared N-doped TiO_2 with alkylammonium salts. They assigned the peak at 400 eV to N in Ti–O–N bonding [18]. The above analysis suggested the presence of O–Ti–N structure and the existence of Ti–O–N bonding. In Fig. 3d, the two peaks located at 373.9 eV and 368.1 eV were according with Ag $3d_{3/2}$ and $3d_{5/2}$, indicating that the Ag loading on the TiO_2 surface mainly existed in the form of zero-valence [19]. Nevertheless, the Ag^+ was considerably larger than the Ti^{4+} (1.26 Å as opposed to 0.67 Å), it was difficult to fit into the TiO_2 lattice [5]. The C 1s peak appearing at 284.7 eV was attributed to graphite [20].

XRD patterns of TC, NTC, NATC and PNATC obtained at different pyrolysis temperatures were shown in Fig. 4. There was no obvious peak of crystalline graphite at 26.8°, suggesting that the graphite phase existed in the out of order structure. When PNATC was pyrolyzed at 700 °C (Fig. 4e), a slender peak appeared at 26.8°, demonstrating that the out of order structure of graphite translated into order structure at 700 °C. Five peaks at 25.4°, 38.3°, 48.0°, 54.4° and 63.1° were attributed to the diffraction of (101), (004), (200), (211) and (204) planes of anatase, respectively [21]. In Fig. 4 (a) and (b), the crystallization pyrolyzing at 600 °C was not obvious, while NATC (Fig. 4c) pyrolyzing at the same temperature showed a typical anatase peak. When NATC doped with SiO_2 was pyrolyzed at 700 °C, the peak of anatase TiO_2 was noticed. The reason is that the crystal temperature increases for the dopant of SiO_2 nano-particles. No significant characteristic peaks of silver oxide were detected, indicating the formation of no silver oxide phase. The crystal sizes of TiO_2 were calculated by the Debye–Scherrer equation from the peak of 25.4° and the results were shown in Table 1. The crystalline size of anatase decreased rapidly with the Ag ion loading. This could be due to silver located at interstitial site of TiO_2, which inhibited the growth of crystal grains.

The Raman spectra of TC and NATC were shown in Fig. 5. Five typical peaks of anatase TiO_2: E_g (150 cm^{-1}), E_g (200 cm^{-1}), B_{1g} (397 cm^{-1}), A_{1g} (517 cm^{-1}) and E_g (629 cm^{-1}) could be found in the figure (shown in the inset of Fig. 5). In contrast to Fig. 5 (a), in which the Eg mode was at 146 cm^{-1}, the Eg mode in Fig. 5 (b) shifted by 4 cm^{-1} toward higher wavelengths. This was likely caused by the formation of Ti–O–N structure in the NATC [22]. The peak of Fig. 5 (b) at

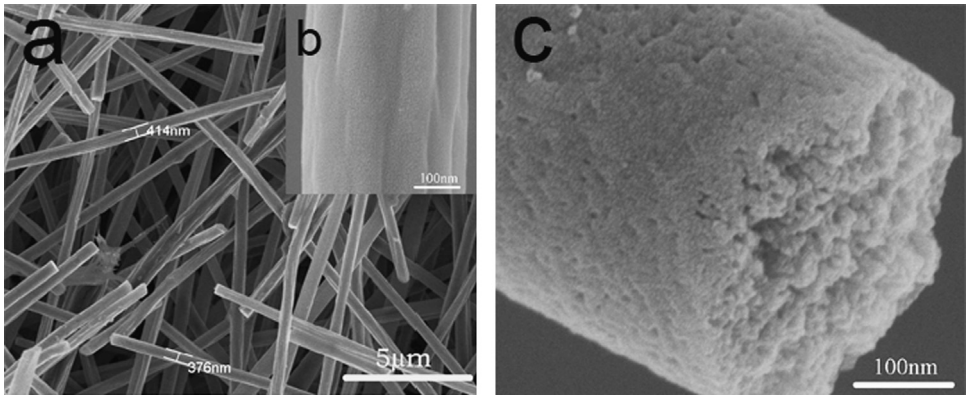

Fig. 1. SEM images of (a, b) NATC fibers, and (c) PNATC fibers.

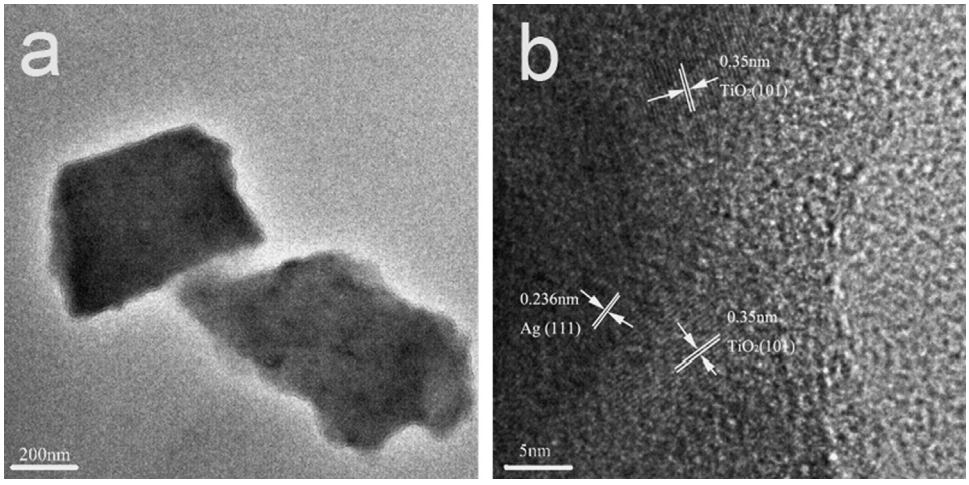

Fig. 2. (a) a typical TEM image and (b) a HRTEM image of NATC.

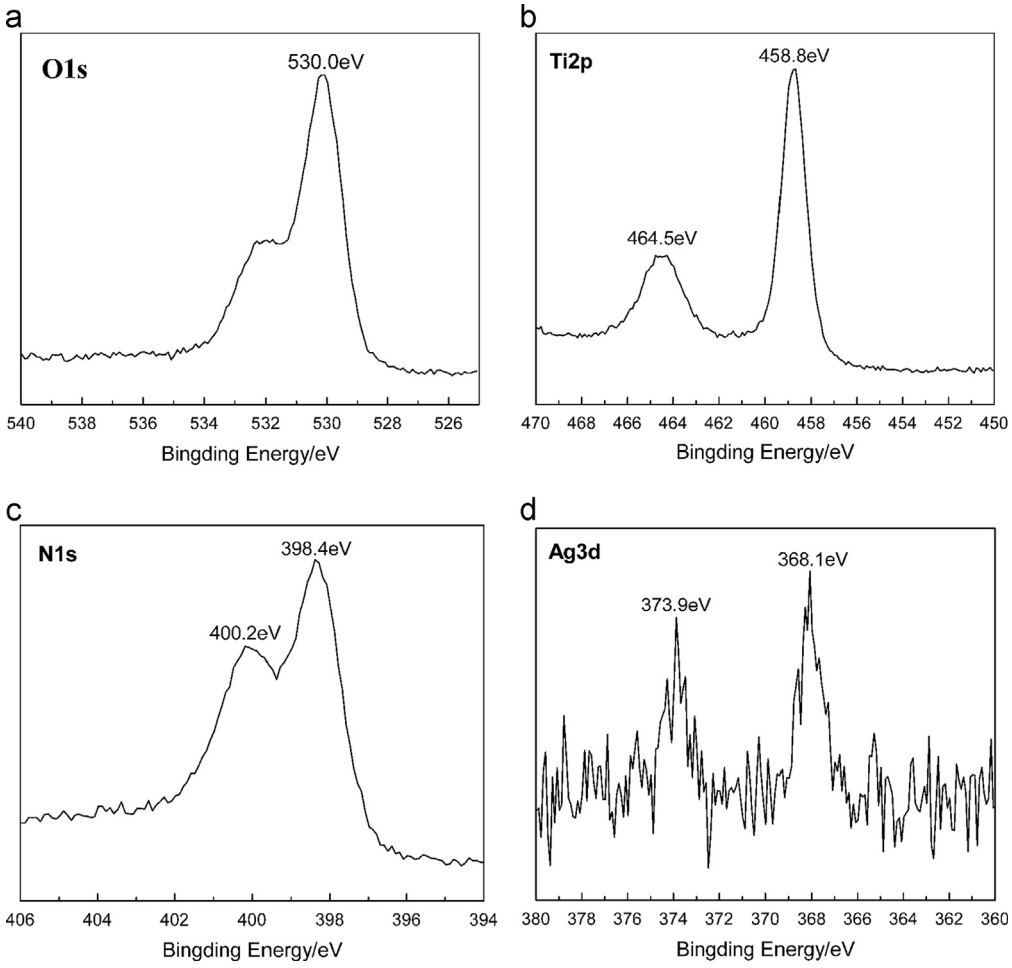

Fig. 3. XPS spectra of (a) O 1s, (b) Ti 2p, (c) N 1s, and (d) Ag 3d for NATC.

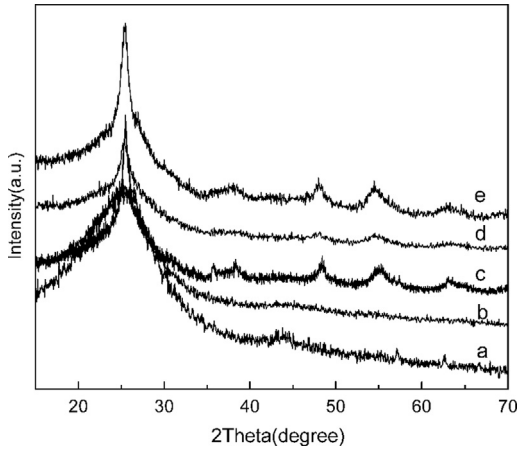

Fig. 4. XRD patterns of (a) TC, (b) NTC, (c) NATC, (d) PNATC-600, and (e) PNATC-700 (600 and 700 represent the pyrolysis temperature).

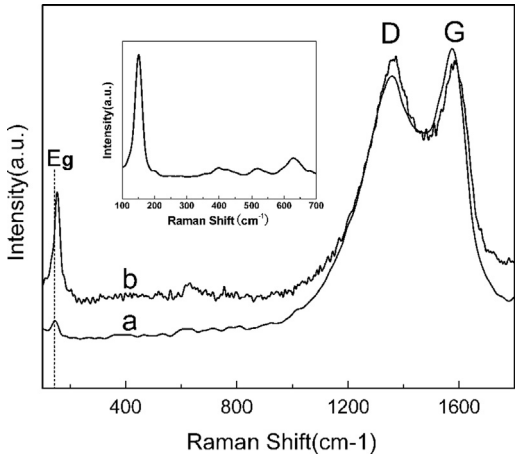

Fig. 5. Raman spectra of (a) TC and (b) NATC. The inset is the enlarged curves of NATC between 100 and 800 cm^{-1}.

150 cm^{-1} was sharper than Fig. 5 (a), demonstrating the crystallization of anatase in NATC was better than that in TC. The result was accordant with XRD patterns, indicating that the crystallinity was enhanced when TC doped with N and Ag. Two broad peaks centered at 1360 and 1581 cm^{-1} were attributed to disordered carbon and ordered graphite domain [23].

The schematic diagram of the formation mechanism of PNATC was demonstrated in Fig. 6. After etching SiO_2 by HF, the final fibers with large number of holes were fabricated.

Fig. 7 presents the nitrogen adsorption–desorption isotherms and Barret–Joyner–Halenda (BJH) pore size distribution curve (in the inset) of PNATC. It exhibited the typical type-IV

Table 1
Crystalline size of samples.

Sample	TC	NTC	NATC	PNATC-600	PNATC-700
Crystalline size (nm)	34.6	37.6	14.2	13.7	11.8

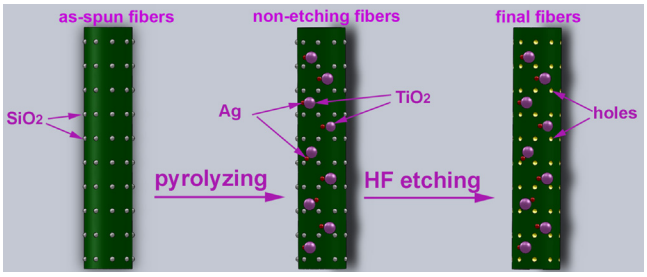

Fig. 6. The schematic diagram represents the formation mechanism of PNATC.

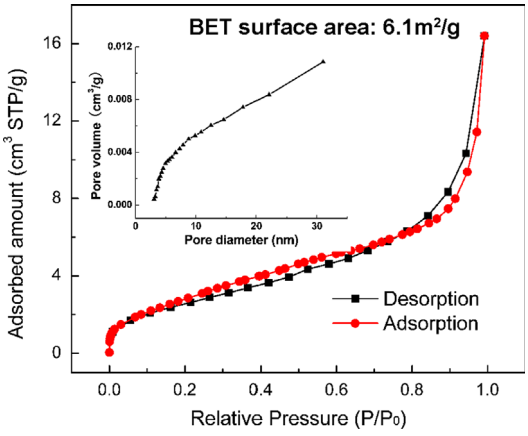

Fig. 7. Nitrogen adsorption–desorption isotherms and pore size distribution curve (inset) of PNATC.

isotherm with a N_2 hysteresis loop for the relative pressure P/P_0 in the range 0.7–1.0, suggesting the presence of mesopores in PNATC. According to the Brunauer–Emmett–Teller (BET) analysis, the surface area of PNATC was 6.1 m^2/g. In addition, the pore size distribution curve was obtained by the BJH method. The pore volume enlarged with the increasing of the pore diameter, indicating a relatively wide pore size distribution at mesopores range. This was relevant to the aggregation of SiO_2 nano-particles.

The UV–vis diffuse reflectance spectra of TC, NTC, NATC and PNATC (pyrolyzed at 600 and 700 °C) shown in Fig. 8. It is apparent that the absorbance of all the samples was above 1.1% including visible light absorption, which was related to the high amount of carbon in the fibers mat. The absorbance of NATC was stronger than that of TC and NTC, indicating that the presence of Ag particles caused apparent enhancement of absorbance in visible light [19]. The porous fibers mat demonstrated a higher absorption at all the ranges (Fig. 8-d and -e). Furthermore, the UV–vis diffuse reflectance spectra of all the samples did not improve too much, suggesting that the

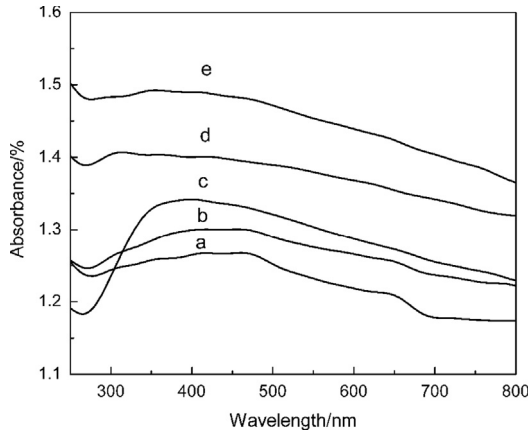

Fig. 8. Diffuse reflectance spectra of (a) TC, (b) NTC, (c) NATC, (d) PNATC-700, and (e) PNATC-600 (600 and 700 represent the pyrolysis temperature).

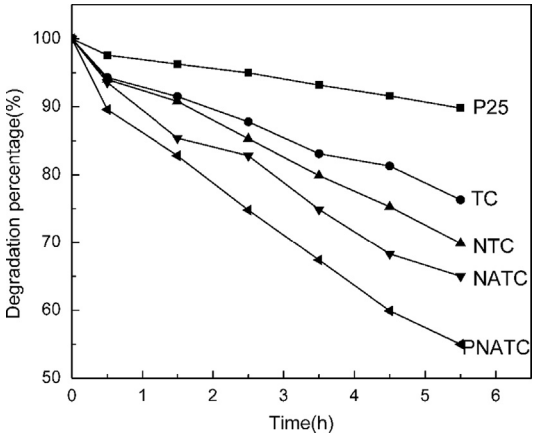

Fig. 9. Photocatalytic activities of P25, TC, NTC, NATC and PNATC mixed with aqueous MB of 10 ppm under visible irradiation ($\lambda > 420$ nm), no visible light irradiation before 0.5 h.

fibers mat consisting of N–Ag co-doped TiO_2 possessed better visible-light absorption ability.

The photocatalytic activities of the fibers mat and P25 were investigated by detecting the remaining concentration of methylene blue (MB) aqueous solution at various time intervals. The MB degradation percentage of different photocatalysts was shown in Fig. 9. The order of visible-light photocatalytic activity was PNATC > NATC > NTC > TC > P25. The highest photocatalytic activity was observed for PNATC (45.1%). According to the TG analysis, there was a total weight loss of 76% from room temperature to 600 °C in air. The carbon element has been removed at 600 °C, indicating that the mass ratio of TiO_2 in NATC was 24 wt%. Silver nano-particles could inhibit the recombination of the photogenerated electron–hole pairs, inducing the photocatalytic efficiency of NATC higher than NTC.

Nevertheless, the fibers mats exhibited higher photocatalytic activity than P25 (consisting of 80% anatase and 20% rutile) under visible light irradiation. Dopants of N–Ag and the adsorption of ultrafine carbon fibers played active roles on enhancing the photocatalytic activity. NATC and NTC demonstrated an enhanced visible-light photocatalytic activity comparing with TC and P25. The reason is that N–Ag co-doping induced the red shift of the absorption edge of TiO_2, narrowing the band gap and enhancing visible-light absorption [21]. The adsorption efficiency of PNATC was twice higher than NATC, NTC and TC for the sample obtained at 0.5 h without visible-light irradiation. The results came from the formation of nano-sized pores after removing SiO_2. This improved the contact area and reacting time between MB and TiO_2, leading the photocatalytic activity of PNATC much higher than the other photocatalysts.

4. Conclusion

N–Ag co-doped TiO_2/C ultrafine fibers mat with porous structure has been prepared by a sol–gel/electrospinning method. TiO_2 distributed in the fibers regularly in anatase phase with the pyrolysis temperature of 700 °C. The adherent Ag mainly existed in the form of zero-valence. However, the N–Ag co-doped TiO_2/C porous fibers mat showed much higher photocatalytic activity for the degradation of methylene blue solution than P25 under visible light. This was concerned to the dopants of N–Ag and high adsorption ability relying on porous carbon fibers. The in-situ synthesis of N–Ag co-doped TiO_2/C fibers mat kept in shape after photocatalytic degradation experiment, which was convenient to reclaim.

Acknowledgment

The authors thank Xin Long and Yan Xu for their help in the measurement of photocatalytic activities. The project was funded by National Natural Science Foundation of China (Nos. 51173202 and 51203182).

References

[1] X.Z. Shen, J. Guo, Z.C. Liu, S.M. Xie, Visible-light-driven titania photocatalyst co-doped with nitrogen and ferrum, Applied Surface Science 254 (2008) 4726–4731.
[2] Y. Cong, J.L. Zhang, F. Chen, M. Anpo, Preparation, photocatalytic activity, and mechanism of nano-TiO_2 co-doped with nitrogen and iron (III), Journal of Physical Chemistry C 111 (2007) 10618–10623.
[3] X.B. Chen, C. Burda, The electronic origin of the visible-light absorption properties of C-, N- and S-doped TiO_2 nanomaterials, Journal of the American Chemical Society 130 (2008) 5018–5019.
[4] H.X. Meng, B.B. Wang, S. Liu, R.Y. Jiang, Hydrothermal preparation, characterization and photocatalytic activity of TiO_2/Fe–TiO_2 composite catalysts, Ceramics International 39 (2013) 5785–5793.
[5] Y. Zhou, K.L. Huang, Z.P. Zhu, B. Yang, C.B. Xia, H.N. Xiao, Preparation and photocatalysis activity of Eu^{2+}/Gd^{3+} codoped nano-TiO_2 multiplex photocatalyst from sol–gel process catalyzed with acid, Journal of Inorganic Materials 23 (2008) 1085–1088.
[6] D.E. Gu, B.C. Yang, Y.D. Hu, V and N co-doped nanocrystal anatase TiO_2 photocatalysts with enhanced photocatalytic activity under visible light irradiation, Catalysis Communications 9 (2008) 1472–1476.
[7] K.S. Rane, R. Mhalsiker, S. Yinb, T. Satob, Visible light-sensitive yellow $TiO_{2-x}N_x$ and Fe–N co-doped $Ti_{1-y}Fe_yO_{2-x}N_x$ anatase photocatalysts, Journal of Solid State Chemistry 179 (2006) 3033–3044.
[8] Y.X. Liu, J.X. Shi, Q. Peng, Y.D. Li, Self-assembly of ZnO nanocrystals into nanoporous pyramids: high selective adsorption and photocatalytic activity, Journal of Materials Chemistry 22 (2012) 6539–6541.
[9] B. Pant, H.R. Pant, N.A.M. Barakat, M. Park, Carbon nanofibers decorated with binary semiconductor (TiO_2/ZnO) nanocomposites for the effective removal of organic pollutants and the enhancement of antibacterial activities, Ceramics International 39 (2013) 7029–7035.
[10] M.L. Chen, C.S. Lim, W.C. Oh, Photocatalytic effect for TiO_2/ACF composite electrochemically prepared with TNB electrolyte, Carbon Letters 8 (2007) 177–183.
[11] J. Ming, Y.Q. Wu, S. Nagarajan, D.J. Lee, Fine control of titania deposition to prepare C/TiO_2 composites and TiO_2 hollow particles for photocatalysis and lithium-ion battery applications, Journal of Materials Chemistry 22 (2012) 22135–22141.
[12] Y.P. Gao, P.F. Fang, F.T. Chen, Enhancement of stability of N-doped TiO_2 photo- catalysts with Ag loading, Applied Surface Science 265 (2013) 796–801.
[13] C. Liu, N.Z. Bao, Z.H. Yang, Research progresses in the photocatalytic character of TiO_2 doped by transition metal irons, Journal of Catalysis 22 (2001) 215–218.
[14] C.D. Valentin, E. Finazzi, G. Pacchioni, Density functional theory and electron paramagnetic resonance study on the effect of N–F codoping of TiO_2, Chemistry of Materials 20 (2008) 3706–3714.
[15] H.Y. Wei, Y.S. Wu, N. Lun, F. Zhao, Preparation and photocatalysis of TiO_2 nanoparticles co-doped with nitrogen and lanthanum, Journal of Materials Science 39 (2004) 1305–1308.
[16] O. Diwald, R.L. Thompson, V. Zubkov, Photochemical activity of nitrogen doped rutile TiO_2 (110) in visible light, Journal of Physical Chemistry B 108 (2004) 6004–6008.
[17] R. Asahi, T. Morikawa, Nitrogen complex species and its chemical nature in TiO_2 for visible-light sensitized photocatalysis, Chemical Physics 339 (2007) 57–63.
[18] G.L. Gole, J.D. Stout, Highly efficient formation of visible light tunable TiO_{2-x} N_x photocatalysts and their transformation at the nanoscale, Journal of Physical Chemistry B 108 (2004) 1230–1240.
[19] S. Sena, S. Mahantya, S. Roya, O. Heintz, Investigation on sol–gel synthesized Ag-doped TiO_2 cermet thin films, Thin Solid Films 474 (2005) 245–249.
[20] X.B. Yan, T. Xu, G. Chen, H.W. Liu, S.R. Yang, Effect of deposition voltage on the microstructure of electrochemically deposited hydrogenated amorphous carbon films, Carbon 42 (2004) 3103–3108.
[21] L.H. Huang, C. Sun, Y.L. Liu, Pt/N-codoped TiO_2 nanotubes and its photo-catalytic activity under visible light, Applied Surface Science 253 (2007) 7029–7035.
[22] G. Liu, C.H. Sun, L.N. Cheng, Y.G. Jin, H.F. Lu, Efficient promotion of anatase TiO_2 photocatalysis via bifunctional surface-terminating Ti–O–B–N structures, Journal of Physical Chemistry C 113 (2009) 12317–12324.
[23] S.J. Yang, S.H. Nam, T.H. Kim, J.H. Im, Preparation and exceptional lithium anodic performance of porous carbon-coated ZnO quantum dots derived from a metal–organic framework, Journal of the American Chemical Society 135 (2013) 7394–7397.